Mechanical Properties and Transparency of Injection-Molded Polyacetal with Branched and Linear Structure: Influence of Crystalline Morphology

Kuniaki Kawaguchi

Research and Development Center, Polyplastics Co., Ltd., 973, Miyajima, Fuji, Shizuoka 416-8533, Japan

Received 16 May 2005; accepted 7 November 2005
DOI 10.1002/app.23777
Published online in Wiley InterScience (www.interscience.wiley.com).

ABSTRACT: Branched and linear polyacetals prepared by cationic bulk polymerization were molded under high-injection rate and pressure, and the resultant 1-mm-thick specimens were investigated regarding the crystalline morphology, mechanical properties, and transparency. The branched polyacetal exhibited shear-induced transformation of crystalline morphology, namely, the spherulites, the elongated spherulites, and shish-kebab morphology parallel to the flow direction, with increasing shear viscosity. The degree of orientation of the branched polyacetal, calculated from the intensity distribution on the Debye ring of the (100) diffraction by WAXS, linearly and significantly increased with the increase of the logarithm of the shear viscosity. The difference of the crystalline morphology greatly influenced the mechanical properties and transparency of the branched and linear polyacetals. The branched polyacetal with the shish-kebab morphology had approximately 20% higher tensile strength and modulus as compared with those with the spherulites morphology, and showed translucent with a higher light transmittance over a wide range of wavelength of incident light. The results indicate that a large number of fibrous crystals in the shish-kebab morphology result in the self-reinforcement of specimens parallel to the flow direction and diminishment of the scattering of incident light. J Appl Polym Sci 100: 3382–3392, 2006

Key words: branched; shear; morphology; mechanical properties; transparency

INTRODUCTION

Polyacetal (alternatively called polyoxymethylene, POM, or acetal resin) is a major engineering thermoplastic widely used in automotive, electrical, electronics, and many industrial field owing to its excellent mechanical properties, abrasion-resistance properties, and processing properties. To further modify its properties, branched polyacetal (alternatively called long-chain branched polyacetal or weakly crosslinked polyacetal) has been experimentally and industrially obtained via the cationic polymerization of 1,3,5-trioxane and ethylene oxide or a cyclic formal in the presence of multifunctional compounds such as diglycidylether or diepoxide,[1–5] and via the anionic polymerization of formaldehyde in the presence of trifunctional or tetrafunctional alcoholic compounds as chain-transfer agents.[6,7] Investigation of branched polyacetal has been undertaken regarding the rheological and crystallization properties. Wissbrun et al.[8] reported the rheological properties of branched polyacetal and its application to blow molding. They indicated that the polymer had a higher viscosity at low shear rates than a linear one, although it had a lower viscosity at high shear rates. Prichard et al.[3] researched the rheological behavior of the branched polyacetal under shear deformation in melt. They reported that the application of shear to the polymer melts consistently raised the melt flow rate while the inherent viscosity remained unchanged, and this flow properties attained steady value after sufficient shearing. They speculated that the flow rate changes caused shear-induced changes in the state of entanglement or aggregation of the polymer chains. Kern et al.[9] reported that branched polyacetal compounds had smaller spherulites and had a higher mechanical strength as compared with linear polyacetal compounds. Thus, the branched structure possesses significant and extra effect on flow properties and is expected to play an important role in controlling the crystalline morphology of polyacetal.

Recently, we reported on the crystalline morphology of injection-molded specimens, 1-mm in thickness, of the branched and linear polyacetals, which were molded under high-injection rate and pressure.[10] This study showed that the specimen of the branched polyacetal with a higher molecular weight had shish-kebab morphology with the formation of fibrous crystals that abounded in an extended chain crystal (ECC). By contrast, the linear polyacetal with a higher molecular weight had no or very few fibrous crystals in the specimens. Wide angle and small angle X-ray scatter-

Correspondence to: K. Kawaguchi (kuniaki.kawaguchi@polyplastics.com).

ing (WAXS and SAXS) results indicated that a specimen with shish-kebab morphology possessed higher degree of orientation along a molding direction as compared with a linear one that had a higher molecular weight. The results strongly suggest that the branched structure of polymer chains, as well as molecular weight, has a significant influence on the formation of the shish-kebab morphology of the injection-molded polyacetal.

Investigation of various properties of the branched and linear polyacetals with different crystalline morphology is useful for the comprehensive development of polyacetal with excellent properties. This article focuses on the crystalline morphology of the injection-molded polyacetal with branched and linear structure, and reports on its influence on the mechanical properties and transparency based on capillary rheometer measurement, scanning electron microscopy (SEM), X-ray scattering, differential scanning calorimetry (DSC), tensile test, dynamic mechanical analysis (DMA), haze value measurement, and UV–visible–NIR spectroscopy.

EXPERIMENTAL

Preparation of polyacetal samples

To prepare the branched polyacetal, the cationic polymerization of 1,3,5-trioxane with 1,3-dioxolane (DOX) was carried out in the presence of a small amount of multifunctional glycidylether by using boron trifluoride as a catalyst. A continuous-type reactor was used for the polymerization, and the reactor temperature was controlled to 80°C. In the polymerization, DOX was used for the insertion of an occasional carbon-to-carbon linkage in the polymer chain for the thermal and chemical stability of polymers. Three multifunctional glycidylether, namely, pentaerythritol polyglycidylether (PGE, epoxy equivalent weight: 231 g/eq), tetramethyleneglycol diglycidylether (TGE, epoxy equivalent weight: 244 g/eq), and hydroquinone diglycidylether (HGE, epoxy equivalent weight: 112 g/eq), were used as branching agents. A small amount of dimethoxymethane was used to adjust the molecular weight and shear viscosity as a chain-transfer agent. The linear polyacetal samples were similarly prepared, except for the polymerization, in the absence of multifunctional glycidylether. Discharged raw polymers from the reactor were poured into a triethyl amine aqueous solution and then left overnight at room temperature to deactivate the catalyst. Resultant polymers were posttreated by using an extruder at 200°C to remove unstable hemiformal fractions, and were formed into pellets.

Table I shows the details of prepared polymers, namely, the branched polyacetal samples (B1–B5) with different branching agent species, different DOX amounts or different shear viscosity, and the linear polyacetal samples (L1–L3) with different shear viscosity. The incorporated amounts of DOX and branching agents in polymers ascertained by ^{1}H-NMR analysis regarding samples B1, B2, L1, and L2 were in good agreement with initial fed amounts as reported in the previous article.[10]

TABLE I
Samples of Branched and Linear Polyacetals

Sample	Fed amount of DOX (wt %)	Branching agent	Fed amount of branching agent (wt %)	Melt viscosity[a] (Pa s)
B1[b]	3.4	PGE	8.0×10^{-2}	2.58×10^2
B2[b]	3.4	PGE	8.0×10^{-2}	5.92×10^2
B3	4.0	TGE	1.6×10^{-1}	2.83×10^2
B4	2.0	HGE	5.0×10^{-2}	4.33×10^2
B5	6.7	HGE	5.0×10^{-2}	5.30×10^2
L1[b]	3.4	—	—	2.85×10^2
L2[b]	3.4	—	—	9.54×10^2
L3	3.4	—	—	4.50×10^2

[a] Measured on a capillary rheometer at 190°C and 1.2×10^3 s^{-1}.
[b] Reported in the previous article.[10]

Preparation of injection-molded specimens

Dumb-bell specimens were molded according to ASTM-D638-TypeIV by using a TOSHIBA IS30FP. Specimens were molded under high-injection rate and pressure. The value of constant injection-molding parameters and specimen molding dimensions are as follows:

- Value of constant injection-molding parameters: injection rate, 100 cm^3/s; injection pressure, 200 MPa; cylinder nozzle temperature, 200°C; molding temperature, 40°C; cooling time, 15 s.
- Value of specimen molding dimensions: length over-all, 115 mm; width over-all: 19 mm; length of narrow section: 33 mm; width of narrow section: 6 mm; thickness: 1 mm.

Instrumentation

Shear viscosity data were obtained on a capillary rheometer TOYOSEIKI Capillograph 1B. The experiments were carried out using a capillary of 10 mm long and 1 mm in diameter, at 190°C. The melt viscosity (η) of the polymer pellets at a higher shear rate, i.e., 1.2×10^3 s^{-1}, was measured for an indication of the injection molding. A good correlation between the shear viscosity and the molecular weight measured on gel-permeation chromatography (GPC) was ascertained regarding B1, B2, L1, and L2 as reported in the previous article.[10]

Scanning electron microscopic (SEM) observation was performed with slices taken parallel to the flow direction from the core position of a narrow section of dumb-bell specimens on a HITACHI *S*-4700 at room temperature. Specimens were cut on a diamond microtome, and then they were etched with 50% of sulfuric acid aqueous solution for 2 min at room temperature, to etch an amorphous and/or low crystallinity portion selectively. These specimens were rinsed by distilled water and dried in a vacuum oven, and then they were ion-sputtered with platinum and palladium. Low accelerating voltage of SEM, i.e., 0.5–1.0 kV, was selected to prevent degradation of specimens by an electron beam.

Wide-angle X-ray scattering (WAXS) was performed on a Rigaku Rint1400 with CuKα radiation at an accelerating voltage of 50 kV and a current of 120 mA. The narrow section of dumb-bell specimens was used for the analysis. The degree of orientation (A) was calculated from the intensity distribution on the Debye ring of the (100) diffraction at $2\theta = 22.8^{\circ}$ from the following equation:

$$A(\%) = \frac{360 - \sum W}{360} \times 100 \tag{1}$$

where ΣW ($^{\circ}$) is the sum of the half width of the (100) peak on the Debye ring.

Differential scanning calorimetric (DSC) measurements were performed with slices taken parallel to the flow direction from the core position of the narrow section of dumb-bell specimens on a PerkinElmer DSC-7. About 10 mg of samples was used for these measurements. To prevent thermal oxidative degradation of the samples, all experiments were performed under a nitrogen atmosphere. The samples were heated at 10°C/min up to 200°C to observe the melting point (T_m) and enthalpy of fusion (ΔH_m). The instrument was calibrated with both indium and benzene.

Tensile tests were performed on an Orientech RTM100 at room temperature. Tensile strength at yield, tensile modulus (Young's modulus), and tensile elongation at break were measured at a crosshead speed of 50 mm/min.

Dynamic mechanical analysis (DMA) data were obtained with a Rheometric Scientific Solids Analyzer RSAIII, at a heating rate of 6°C/min and a frequency of 1 Hz. The dumb-bell specimens were used for the analysis. A small three-point bend clamp, whose support-to-support span was 40 mm long, was chosen for this investigation.

Light transmittance, diffuse transmittance, and haze value of specimens (gate side portion) for visible light was measured on a TOYO SEIKI SEISAKU-SHO integration sphere haze-meter at room temperature. The haze value (Haze) is given by

$$\text{Haze } (\%) = \frac{T_d}{T_t} \times 100 \tag{2}$$

where T_t is the light transmittance (%), and T_d is the diffuse transmittance (%).

Light transmittance was further measured on a JASCO V-570 UV–visible–NIR (ultraviolet, visible, and near-infrared) spectrometer equipped with an integrating sphere and a double beam spectrometer with two monochromators. In the spectrometer, the dual detector design incorporated a photomultiplier detector for the UV–visible and a Peltier-cooled lead sulfide (PbS) detector for the NIR region. The measurement was carried out in the wavelength range of 200–2000 nm at room temperature, and the narrow section of dumb-bell specimens was used for the measurement.

RESULTS AND DISCUSSION

Crystalline morphology of branched and linear polyacetals

The difference between the branched and linear polyacetals regarding the crystalline morphology of injection-molded specimens was investigated by using SEM. The samples were etched with 50% of sulfuric acid aqueous solution, to etch an amorphous and/or low crystallinity portion selectively prior to the observation. Figure 1 shows the SEM micrographs at the cross section of injection-molded specimens of the linear polyacetal. The crystalline morphology of the specimens, L1 and L2, has already been reported in the previous article.[10] Specimens of L1 (a), with a lower shear viscosity at 2.85×10^2 Pa s at 1.2×10^3 s^{-1} as an indication of the shear rate of the injection-molding, showed the spherulites morphology; the diameter of the spherulites of L1 was ca. 5–10 μm long. Clark[11,12] and several researchers reported that injection-molded polyacetal specimens had a spherulitic core, and the results of L1 was in agreement with their findings. In the case of L2 (b), with a higher shear viscosity of 9.54×10^2 Pa s, the elongated spherulites morphology was observed at the cross section of the specimen. Fibrous crystals were not clearly observed as shown in the magnified photograph of L2 (c). The crystalline morphology of L3 having a shear viscosity of 4.50×10^2 Pa s was nearly consistent with that of L2, and showed the elongated spherulites morphology with no or very few fibrous crystals. Thus, the linear polyacetal specimens exhibited the transformation of the crystalline morphology from the spherulites to the elongated spherulites with no or very few fibrous crystals, with increasing shear viscosity.

Figure 2 shows the SEM micrographs at the cross section of injection-molded specimens of the branched polyacetal. The crystalline morphology of the speci-

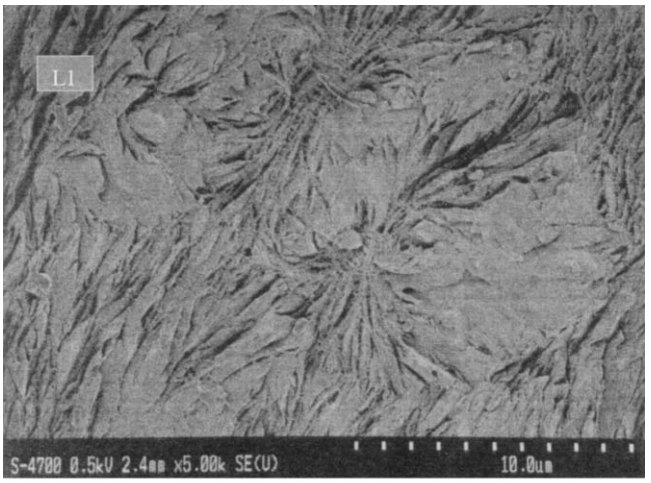

(a)

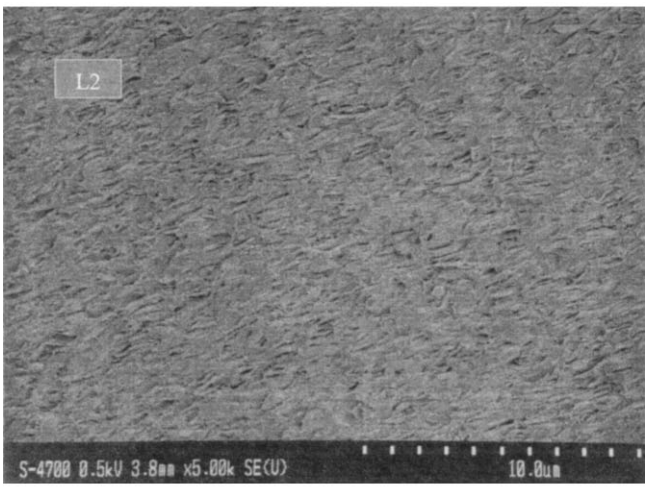

(b)

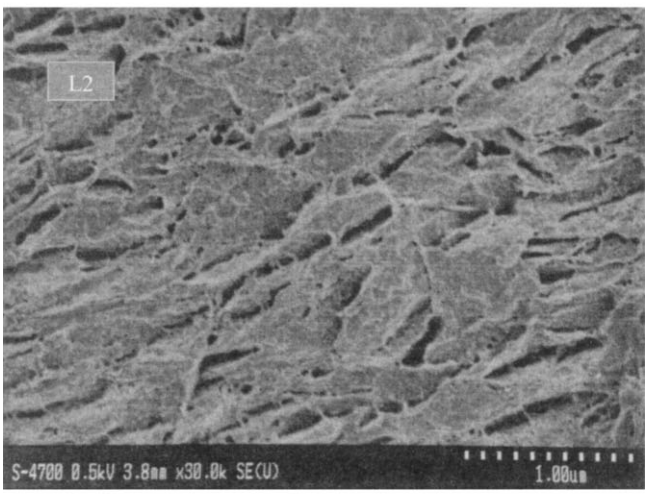

(c)

Figure 1 SEM micrographs at cross section of specimens of linear polyacetal with the molding direction horizontal: (a) L1; (b) L2; (c) magnified photograph of L2.

mens, B1 and B2, has already been reported.[10] The specimens of B1 and B3, with a lower shear viscosity below 3.0×10^2 Pa s, showed the spherulites morphology ((a) and (c)); the diameter of their spherulites was ca. 2 μm long and significantly decreased as compared with that of linear polyacetal L1 [Fig. 1(a)]. These results were consistent with the findings by Kern et al.[9] who reported that branched polyacetal compounds had smaller spherulites. The specimens of B4, with a shear viscosity of 4.33×10^2 Pa s, yielded the elongated spherulites morphology with wavy form at the cross section of the specimen (d), indicating that the spherulites morphology transformed and extended under high-shear stress owing to high-shear viscosity, and the precursor of fibrils was generated along the flow direction. In the case of B2 and B5 having a higher shear viscosity over 5.0×10^2 Pa s, the shish-kebab morphology with a formation of a large number of fibrous crystals was observed parallel to the flow direction ((b) and (e)). Figure 2(f, g) shows the magnified photographs of B2 and B5, respectively. Both specimens had the fibrous crystals of which the width was around 100 nm, and the fibrils were linked to a perpendicular direction with each other and partially coalescent and colligative in the shish-kebab morphology. The observed morphology is expected to be similar to the interlocking shish-kebab structure that was observed by Odell et al.[13–15] in highly oriented polyethylene filaments. From the comparison between B1 and B3, and between B2 and B5, no clear dependence of branching agent species and DOX amounts on the crystalline morphology was observed in these experiments. Table II summarizes the SEM observation results.

The injection-molded specimens of the branched polyacetal exhibited the shear-induced transformation of the crystalline morphology in this way, namely, the spherulites, the elongated spherulites, and the shish-kebab morphology parallel to the flow direction with increasing shear viscosity. The results indicate that the high-shear stress owing to high shear viscosity developed fibrous crystals along the flow direction when they crystallized from the melt, and that the spherulitic structure was transformed to the fibrous structure with increasing shear viscosity. Pople et al.[16] reported that polyethylene subjected to a shear rate above a critical value resulted in macroscopically oriented structures, and the highest molecular weight component affected the formation of fibrous crystals. From the SEM observation results, it is reasonable to consider that a critical shear viscosity exists between the shear viscosity of B4 and B5 to form the shish-kebab morphology in the injection-molded specimens of the branched polyacetal. Figure 3 shows the correlation between the degree of orientation, calculated from the intensity distribution on the Debye ring of the (100) diffraction at $2\theta = 22.8^\circ$ by WAXS, and the logarithm

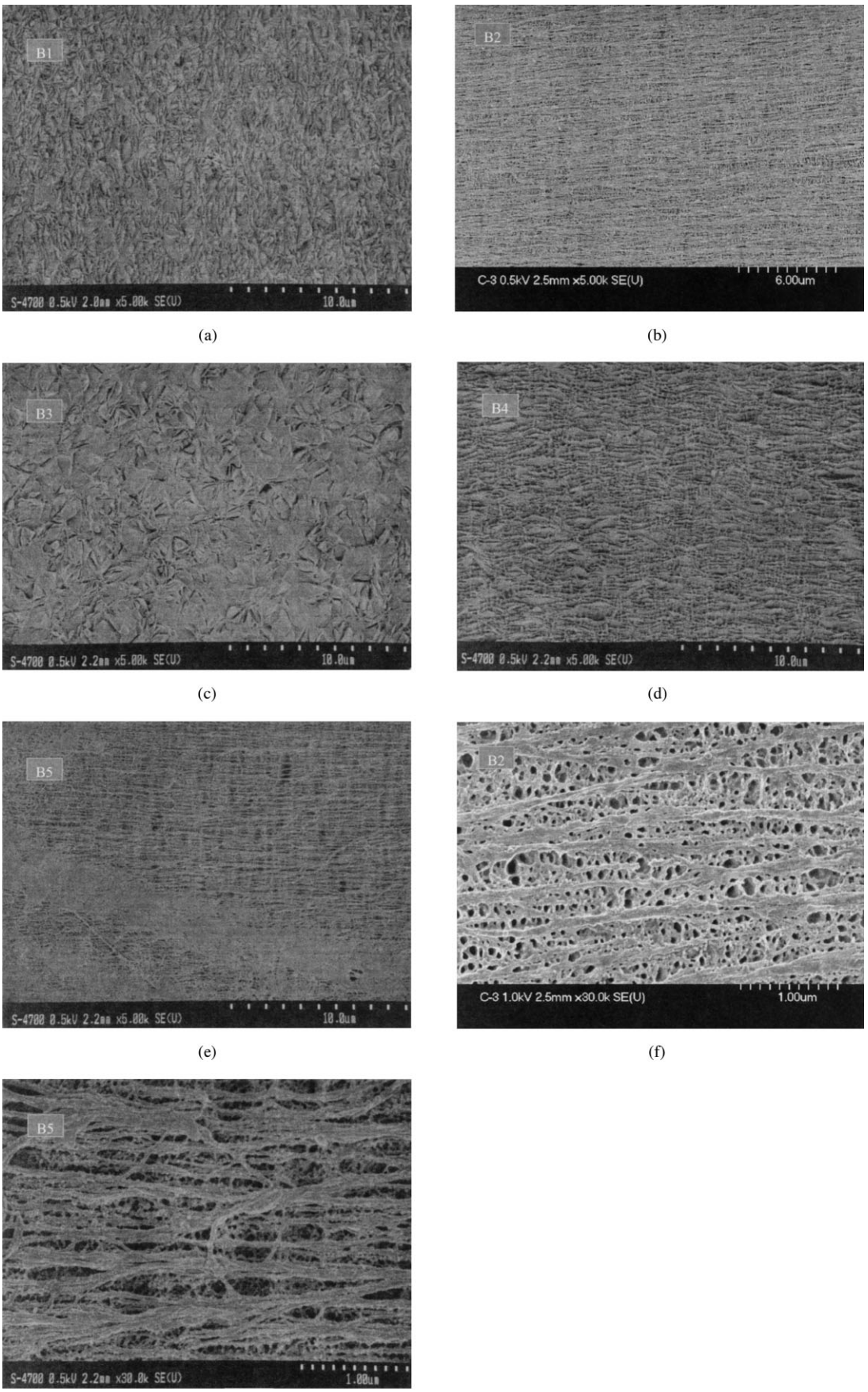

Figure 2 SEM micrographs at cross section of specimens of branched polyacetal with the molding direction horizontal: (a) B1; (b) B2; (c) B3; (d) B4; (e) B5; (f) magnified photograph of B2; (g) magnified photograph of B5.

TABLE II
SEM Observation Results and Degree of Orientation

Specimen	Observed crystalline morphology[a]	Degree of orientation[b] (%)
B1[c]	Spherulites	78.9
B2[c]	Shish-kebab	91.8
B3	Spherulites	79.2
B4	Elongated spherulites (with precursor of fibrils)	85.3
B5	Shish-kebab	90.1
L1[c]	Spherulites	70.1
L2[c]	Elongated spherulites	80.7
L3	Elongated spherulites	75.0

[a] Specimens were cut along the flow direction of the core position of the narrow section.
[b] Calculated from the intensity distribution on the Debye ring of the (100) diffraction at $2\theta = 22.8°$ based on the equation (1).
[c] Reported in the previous article.[10]

of the shear viscosity (log η) at 190°C and 1.2×10^3 s^{-1}, and the data are listed in Table II. The linear relationship was clearly observed for both the branched and linear polyacetals, shown in Figure 3. The degree of orientation of the branched polyacetal significantly increased with the increase of log η, strongly supporting the tendency of the fibrous crystals formation in the polymer as shown in SEM photographs.

Mechanical properties of branched and linear polyacetals

Several research groups reported that highly oriented polyacetal fibers or filaments possessed high strength and modulus properties.[17–19] Moreover, it has been reported that polyolefin is self-reinforced in an injection-molding process under high-shear stress.[20–22] However, few studies have reported on the mechanical properties of injection-molded polyacetal with a higher shear viscosity,[23] especially for the polyacetal with long-chain branched structure. In this section, the influence of crystalline morphology on mechanical properties is discussed, regarding the branched and linear polyacetals.

Tensile strength at yield, tensile modulus (Young's modulus), tensile elongation at break, and thermal data are tabulated in Table III for the branched and linear polyacetals. Figure 4 shows the correlation between the tensile strength and log η. In the case of the branched polyacetal, the tensile strength linearly increased with the increase of log η. The following equation can be established for relating the tensile strength of the branched polyacetal (TS_B) to log η with a correlation coefficient (R^2) 0.95.

$$TS_B(\text{MPa}) = 25.4 \log \eta_B + 4.8 \quad (\text{for } 2.41 \leq \log \eta_B \leq 2.77) \quad (3)$$

where η_B is the shear viscosity (Pa s) of the branched polyacetal, and the value of R^2 is an indication of the quality of linear least squares fit. Figure 5 shows the correlation between the tensile modulus and log η for both the branched and linear polyacetal specimens. Similar to the tensile strength, the tensile modulus of the branched polyacetal (TM_B) also linearly increased with the increase of log η, and was approximately given by the following equation with a correlation coefficient (R^2) 0.97.

$$TM_B(\text{MPa}) = 510.0 \log \eta_B - 148.6 \quad (\text{for } 2.41 \leq \log \eta_B \leq 2.77) \quad (4)$$

The tensile elongation was distributed in the range of ca. 20–30%, and B1 and B3 showed a slightly higher value. The results of tensile strength and modulus indicate that the generated fibrous crystals self-reinforce the specimen along the flow direction with increasing shear viscosity. The specimens with the shish-kebab morphology, B2 and B5, had approximately 20% higher tensile strength and modulus as compared with those with the spherulites morphology, reflecting a large number of fibrous crystals in the shish-kebab morphology parallel to the flow direction.

The plot of the tensile strength versus the degree of crystallinity is shown in Figure 6, and the data are given in Table III. The degree of crystallinity (X_c) is given by the following equation:

$$X_c(\%) = \frac{\Delta H_m}{\Delta H_m{}^0} \times 100 \quad (5)$$

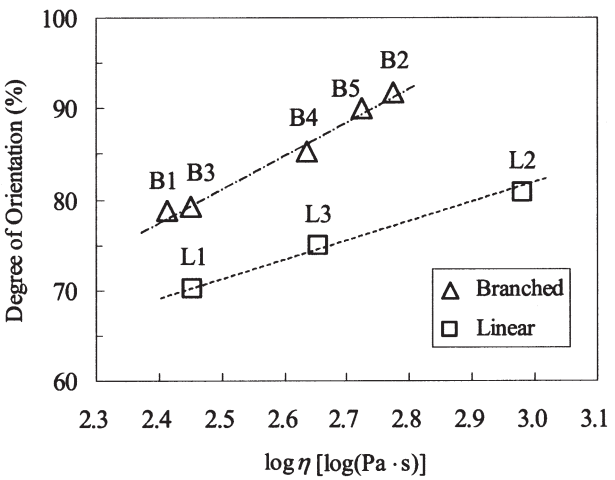

Figure 3 Plot of degree of orientation versus logarithm of shear viscosity (log η) at 190°C and 1.2×10^3 s^{-1} for branched and linear polyacetals.

TABLE III
Mechanical and Thermal Properties of Specimens

Specimen	Tensile strength [at yield] (MPa)	Tensile modulus (MPa)	Tensile elongation (%)	T_m (°C)	ΔH_m (J/g)	X_c [a] (%)
B1	67.3	1096	30.3	165.1	150.2	60.5
B2	75.5	1259	23.9	166.0	145.5	58.6
B3	66.0	1081	26.4	164.3	151.5	61.0
B4	71.2	1204	22.4	169.7	155.0	62.4
B5	74.4	1245	25.5	161.5	129.6	52.2
L1	63.7	1058	41.4	165.1	146.2	58.9
L2	60.8	968	37.3	165.4	132.3	53.3
L3	61.8	997	36.9	165.5	141.2	56.9

[a] Degree of crystallinity calculated from the equation (5).

where ΔH_m^0 is the enthalpy of fusion per gram for 100% crystalline polyacetal, which is assumed to be 248.3 J/g (59.3 cal/g) as reported by Starkweather et al.[24] The inconsistency of the DOX content of the branched polyacetal apparently reflected on the difference of the degree of crystallinity in the specimens. In general, the mechanical strength of semicrystalline polymers correlates to the degree of crystallinity.[25] However, there was an insufficient relationship between the tensile strength and the degree of crystallinity in Figure 8; the specimens of B2 and B5 had a higher tensile strength, although they had a lower degree of crystallinity. This result indicates that the self-reinforcement by the fibrous crystals of B2 and B5 is less accompanied by the increase of crystallinity. In addition, in the case of B4, a slightly higher enthalpy of fusion owing to a lower DOX content, viz., slightly higher crystallinity, as well as self-reinforcement effect, is expected to affect the strength and modulus. Figure 7 shows the DMA results concerning the flexural deformation of the branched polyacetal specimens. Both B1 and B2 had a nearly equivalent loss tangent (tan δ), and B2 had a higher storage modulus (E') and loss modulus (E'') as compared with B1, over a wide range of temperature. Similar to the tensile test result, the higher flexural modulus of B2 is attributed to a large number of fibrous crystals in the specimen perpendicular to the deformation direction.

On the other hand, in Figures 4 and 5, the tensile strength and modulus of the linear polyacetal linearly decreased with the increase of log η. The following equation can be established to relate the tensile strength (TS_L) and modulus (TM_L) of the linear polyacetal to log η with a correlation coefficient (R^2) 0.90 and 0.89, respectively.

$$TS_L\,(\text{MPa}) = -5.3 \log \eta_L + 76.4 \quad (\text{for } 2.45 \le \log \eta_L \le 2.98) \quad (6)$$

$$TM_L\,(\text{MPa}) = -163.4 \log \eta_L + 1448.2 \quad (\text{for } 2.45 \le \log \eta_L \le 2.98) \quad (7)$$

where η_L is the shear viscosity (Pa s) of the linear polyacetal. The tensile elongation of the linear polyac-

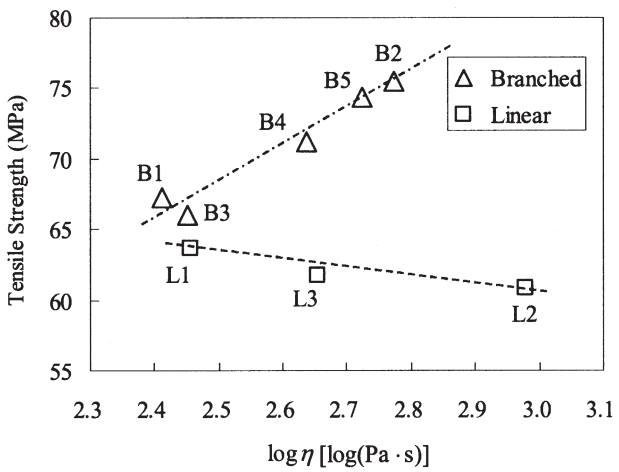

Figure 4 Plot of tensile strength versus logarithm of melt viscosity (log η) at 190°C and $1.2 \times 10^3\ s^{-1}$ for branched and linear polyacetals.

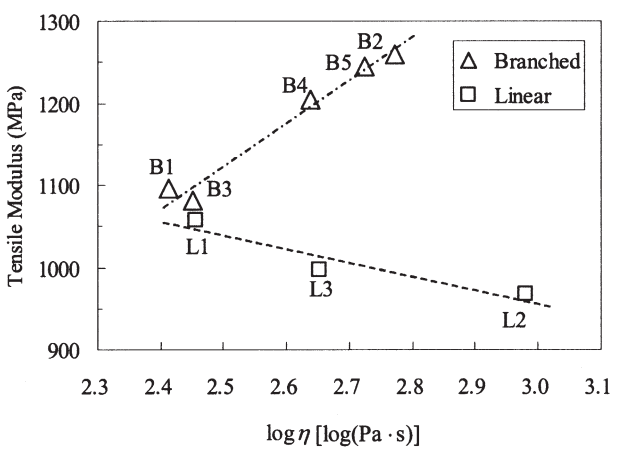

Figure 5 Plot of tensile modulus versus logarithm of melt viscosity (log η) at 190°C and $1.2 \times 10^3\ s^{-1}$ for branched and linear polyacetals.

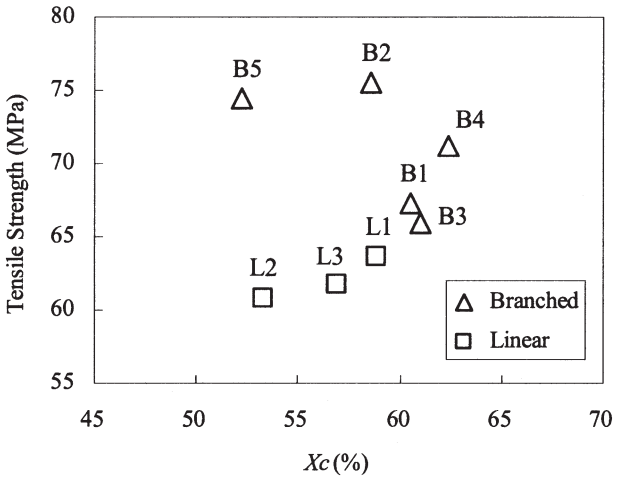

Figure 6 Plot of tensile strength versus degree of crystallinity (X_c) for branched and linear polyacetals.

etal distributed around 40%, and was higher than that of the branched polyacetal. Tanimura et al.[23] also investigated the mechanical properties of the linear polyacetal conforming to ASTM and reported that the flexural modulus of the linear polyacetal specimens decreased with the increase of molecular weight. The differences between the branched and linear polyacetals concerning the strength and modulus is ascribed to the differences of crystalline morphology between both polymers: there are no or very few fibrous crystals in the injection-molded specimens of linear polyacetal with a higher shear viscosity, resulting in no or less self-reinforcement in the specimens parallel to the flow direction. In addition, the decrease of the mechanical strength and modulus of the linear polyacetal with a higher shear viscosity should be attributed to the fact that the high-molecular weight polymer inhibit crystallization and, as a result, lower crystallinity (Fig. 6).

Transparency of branched and linear polyacetals

In spherulites, a large numbers of crystallites grow radially outwards from a nucleus, form an optically anisotropic structure, and generate birefringence. The light-scattering properties of spherulites, and hence the transparency of semicrystalline polymers, are generally dominated not by the fine-scale refractive index fluctuations associated with the alternating crystalline–amorphous morphology, but by the optical properties of the larger spherulitic structure.[26] Coates et al.[18] reported that highly oriented polyacetal filaments became transparent with the increase of the extrusion ratio, reflecting the disappearance of the spherulitic structure in polyacetal filaments. On the other hand, the transparency of injection-molded polyacetal under high-shear processing, especially for the branched polyacetal, has not been well investigated. In this section, the influence of crystalline morphology on the

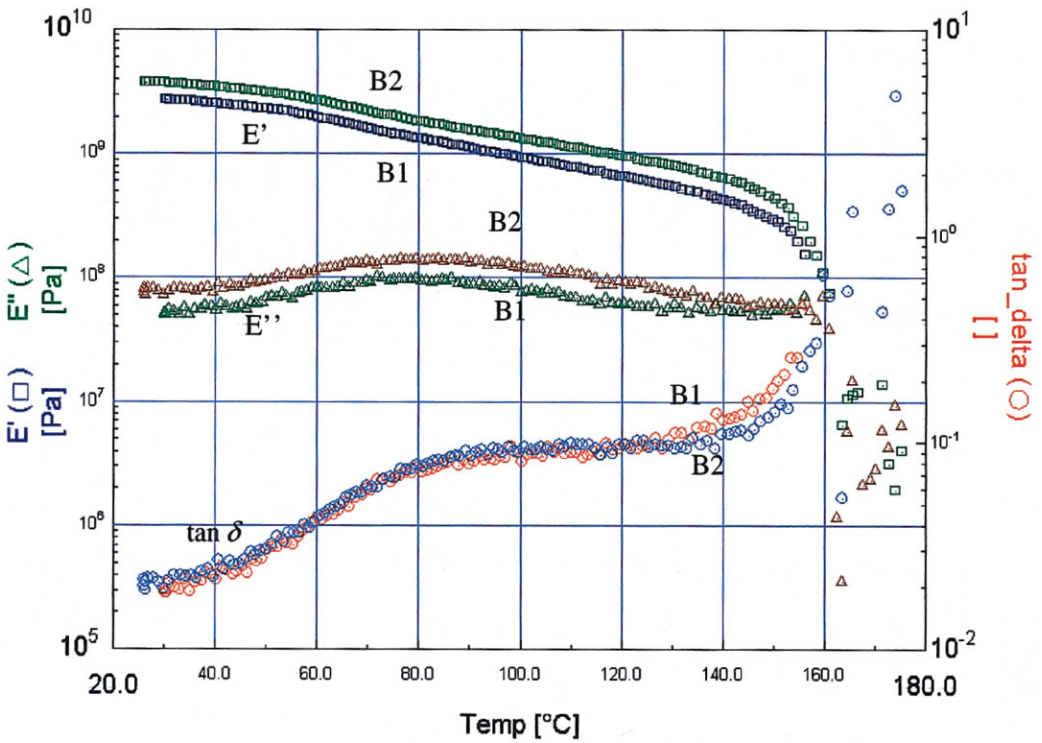

Figure 7 DMA curves at a heating rate of 6°C/min and a frequency of 1 Hz for B1 and B2. [Color figure can be viewed in the online issue, which is available at www.interscience.wiley.com.]

TABLE IV
Optical Properties of Specimens

Specimen	Light transmittance (%)	Diffuse transmittance (%)	Haze value (%)	Optical appearance[a]
B1	53.1	49.8	93.8	Opaque
B2	76.2	52.5	68.9	Translucent
B3	57.7	53.2	92.2	Opaque
B4	66.1	58.8	89.0	Opaque
B5	71.8	50.1	69.8	Translucent
L1	49.6	46.6	94.0	Opaque
L2	72.4	67.2	92.8	Opaque
L3	63.9	59.7	93.4	Opaque

[a] Visual observation results for the narrow section of dumb-bell specimens.

transparency of injection-molded specimens is discussed, regarding the branched and linear polyacetals.

The light transmittance, diffuse transmittance, and haze value of specimens were investigated by using an integration sphere haze-meter. The results are summarized in Table IV. Figure 8 shows the plot of both light transmittance and diffuse transmittance versus log η of the branched polyacetal specimens. The light transmittance of the branched polyacetal linearly increased with the increase of log η. The diffuse transmittance of the branched polyacetal specimens was plotted in the range of ca. 50–60%, and B4 had a maximum diffuse transmittance. Figure 9 shows the plot of both light transmittance and diffuse transmittance versus log η of the linear polyacetal specimens. In this case, both light transmittance and diffuse transmittance curvilinearly increased with the increase of log η, and the diffuse transmittance was close to the light transmittance over a wide range of log η. The results of shear viscosity dependence indicate that the difference of the crystalline morphology greatly influence the transparency of the branched and linear polyacetal specimens. The specimen with the shish-kebab morphology, B2 and B5, had a higher light transmittance, over 70%, versus a lower diffuse transmittance, ca. 50%, indicating that a large number of fibrous crystals diminished the scattering of incident light in the specimens. The specimens with the elongated spherulites morphology, B4, L2, and L3, had a comparatively higher light transmittance; however, they also had a higher diffuse transmittance, and the diffuse transmittance was close to the light transmittance. This phenomenon can be attributed to the fact that the elongated spherulites have a fine but optical heterogeneous structure because of the irregular shape of the crystalline morphology. In the case of the specimens with the spherulites morphology, B1, B3, and L1, diameters of spherulites were larger than the wavelength of incident light; therefore, the scattering of incident light due to the spherulites morphology caused a lower light transmittance, and the diffuse transmittance was close to the light transmittance.

Figure 10 shows the plot of the haze value versus log η of both the branched and linear polyacetal specimens. The haze value was calculated from the percentage of the diffuse transmittance to the light transmittance; therefore, those of the linear polyacetal kept an almost constant value over 90% versus log η. On

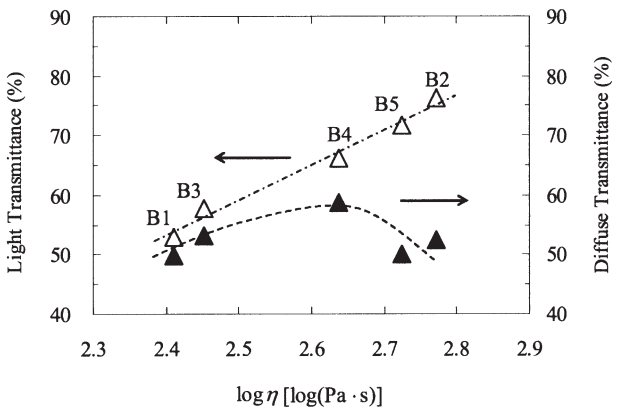

Figure 8 Plot of light transmittance and diffuse transmittance versus logarithm of melt viscosity (log η) at 190°C and 1.2×10^3 s^{-1} for branched polyacetal.

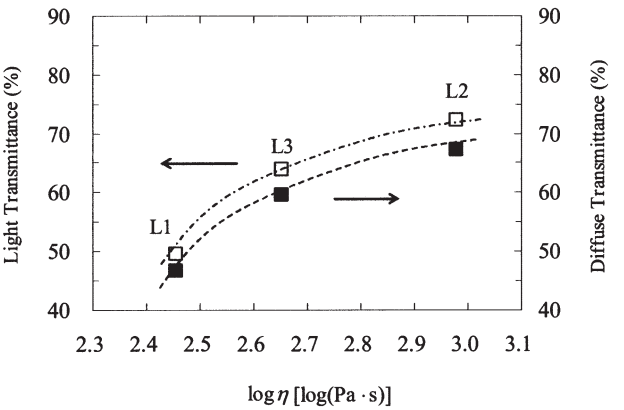

Figure 9 Plot of light transmittance and diffuse transmittance versus logarithm of melt viscosity (log η) at 190°C and 1.2×10^3 s^{-1} for linear polyacetal.

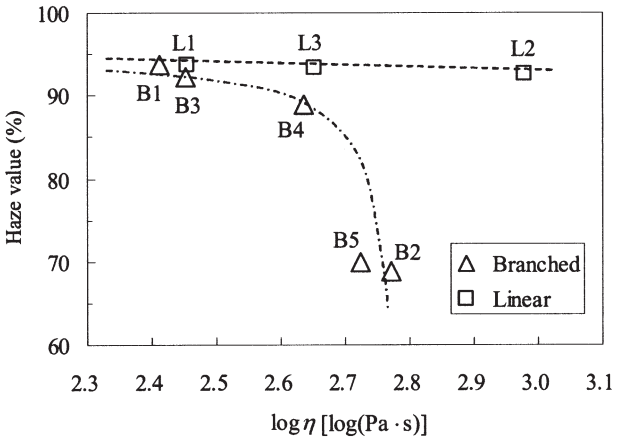

Figure 10 Plot of haze value versus logarithm of melt viscosity (log η) at 190°C and $1.2 \times 10^3\ s^{-1}$ for branched and linear polyacetals.

the other hand, the haze value of the branched polyacetal specimens drastically decreased or jumped from ca. 90 to 70%, when log η increases from ca. 2.6 to 2.8; the specimens with the shish-kebab morphology, B2 and B5, had a lower haze value among these samples. The optical appearance of the narrow section of dumb-bell specimens was directly evaluated by visual observation. The results are listed in Table IV. The specimen of B2 and B5, with the shish-kebab morphology, showed translucent, whereas others showed opaque, strongly supporting the results of the haze value measurement. Examples of specimens (gate side and narrow section), B1 and B2, are shown in Figure 11. The specimen of B2 clearly showed translucent in contrast to the opaqueness and whiteness of the specimen of B1.

The light transmittance of the branched polyacetal was further investigated by using an UV–visible–NIR spectrometer over a wide wavelength range of incident light, i.e., UV region from 200 to 400 nm, visible light region from 400 to 800 nm, and NIR region from

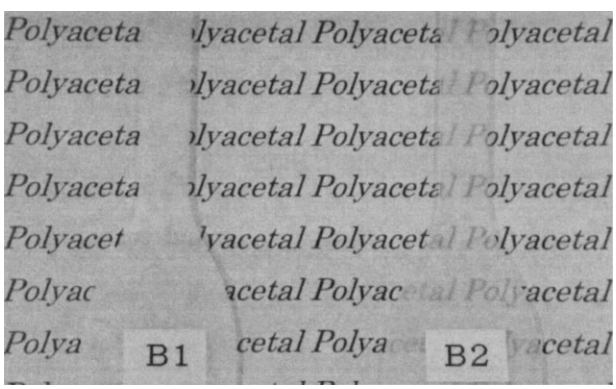

Figure 11 Optical appearance of injection-molded specimens: B1 and B2.

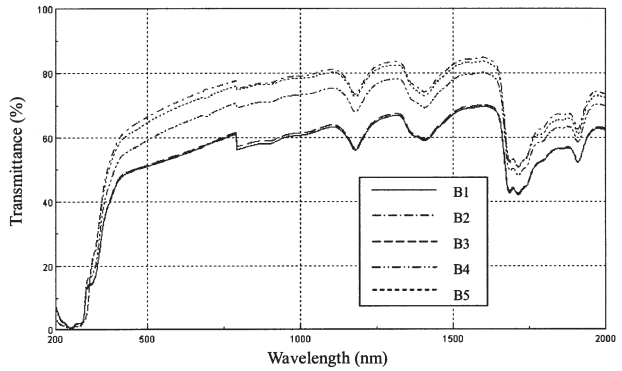

Figure 12 UV–visible–NIR spectra of branched polyacetal.

800 to 2000 nm. Figure 12 shows the UV–visible–NIR spectra of the branched polyacetal specimens versus the wavelength of incident light. In the spectra, baseline jump was observed at 800 nm, because both gratings and detectors in a spectrometer were exchanged automatically between the visible light and the NIR region. The light transmittance decreased with the decrease of the wavelength of incident light in the visible light region, and the trend was substantially similar for all samples. In the UV region, the light transmittance of these specimens drastically decreased, and the light transmittance below 300 nm of wavelength was hardly detected. In the NIR region, characteristic absorption bands attributed to the chemical structure of polyacetal were observed over a wide range. The specimens with the shish-kebab morphology, B2 and B5, had a higher light transmittance over a wide range of wavelength of incident light. By contrast, the specimens with the spherulitic morphology, B1 and B3, had a lower light transmittance, and the specimens with the elongated spherulites morphology, B4, had an in-between value among all specimens. The results substantiate that differences in the crystalline morphology greatly influence the light transmittance of the branched polyacetal specimens over a wide range of wavelength of incident light.

CONCLUSIONS

The difference between the branched and linear polyacetal regarding the mechanical properties and transparency of the injection-molded specimens was investigated and the results were discussed from the viewpoint of crystalline morphology. The injection-molded specimens of the branched polyacetal exhibited the shear-induced transformation of the crystalline morphology, namely, the spherulites, the elongated spherulites, and the shish-kebab morphology parallel to the flow direction, with increasing shear viscosity. By contrast, the linear polyacetal specimens exhibited the transformation of the crystalline morphology from

the spherulites to the elongated spherulites with no or very few fibrous crystals, with increasing shear viscosity. The degree of orientation of the branched polyacetal, calculated from the intensity distribution on the Debye ring of the (100) diffraction by WAXS, linearly and significantly increased with the increase of the logarithm of the shear viscosity (log η). From the comparison between B1 and B3, and between B2 and B5, no clear dependence of branching agent species and DOX amounts on the crystalline morphology was observed.

The difference of the crystalline morphology greatly influenced the mechanical properties and transparency of the branched and linear polyacetals. The specimens with the shish-kebab morphology, B2 and B5, had approximately 20% higher tensile strength and modulus as compared with those with the spherulites morphology, B1 and B3, although B2 and B5 had a lower degree of crystallinity. DMA results indicate that B2 had a higher storage modulus (E') and loss modulus (E'') as compared with B1 over a wide range of temperature. Furthermore, the specimens B2 and B5 showed translucent and had a higher light transmittance over a wide range of wavelength of incident light. The results indicate that a large number of fibrous crystals in the shish-kebab morphology result in the self-reinforcement of specimens parallel to the flow direction, and diminish the scattering of incident light in the specimens.

The long-chain branched structure in polyacetal plays an important role in generating these unique crystalline morphology and properties via high-shear deformation in melt, and the results provide possibilities to further and comprehensively improve the performance of conventional polyacetal. In this work, the crystalline morphology was studied for the core portion of the injection-molded specimens. It is interesting to compare the results with those obtained for a skin layer or an intermediate layer of the specimens, to further clarify the influence of the crystalline morphology on the mechanical properties and transparency.

The author expresses his gratitude to many colleagues in Polyplastics Co., Ltd. for help and advice.

References

1. Weissermel, K.; Fischer, E.; Gutweiler, K.; Hermann, H. Kunststoffe 1964, 54, 410.
2. Park, I. K. Makromolek Chem 1968, 118, 375.
3. Prichard, J. H.; Wissbrun, K. F. J Appl Polym Sci 1969, 13, 233.
4. Heinz, W. E.; McAndrew, F. B. Jap. Pat. 45–25114 (1970).
5. Mateva, R.; Sirashki, G.; Glavchev, I. J Appl Polym Sci 1996, 61, 2151.
6. Matsuzaki, K.; Masamoto, J. Jap. Pat. 60–54985 (1985).
7. Nagasaki, K.; Hata, T.; Matsuzaki, K. Polym Prepr Japan 1990, 39, 253.
8. Wissbrun, K. F. Polym News 1977, 4, 55.
9. Kern, R.; Schmidt, H.; Burg, K. H.; Wolters, E.; Sextro, G. Jap. Pat. 55–19942 (1980).
10. Kawaguchi, K.; Tajima, Y. Kobunshi Ronbunshu 2005, 62, 124.
11. Clark, E. S. Appl Polym Symp 1973, 20, 325.
12. Clark, E. S. Appl Polym Symp 1974, 24, 45.
13. Odell, J A.; Grubb, D. T.; Keller, A. Polymer 1978, 19, 617.
14. Bashir, Z.; Odell, J. A.; Keller, A. J Mater Sci 1984, 19, 3713.
15. Bashir, Z.; Odell, J. A.; Keller, A. J Mater Sci 1986, 21, 3993.
16. Pople, J. A.; Mitchell, G. R.; Sutton, S. J.; Vaughan, A. S.; Chai, C. K. Polymer 1999, 40, 2769.
17. Clark, E. S.; Scott, L. S. Polym Eng Sci 1974, 14, 682.
18. Coates, P. D.; Ward, I. M. J Polym Sci Polym Phys 1978, 16, 2031.
19. Hope, P. S.; Richardson, A.; Ward, I. M. J Appl Polym Sci 1981, 26, 2879.
20. Maertin, C.; Ehrenstein, G. W. Soc Plast Eng Annu Tech Conf 1987, 45, 816.
21. Guan, Q.; Zhu, X.; Chiu, D.; Shen, K.; Lai, F. S.; McCarthy, S. P. J Appl Polym Sci 1996, 62, 755.
22. Guan, Q.; Lai, F. S.; McCarthy, S. P.; Chiu, D.; Zhu, X.; Shen, K. Polymer 1997, 38, 5251.
23. Tanimura, N.; Nanasawa, A.; Polym Prepr Japan 2001, 50, 545.
24. Starkweather, H. W.; Boyd, R. H. J Phys Chem 1960, 64, 410.
25. Schultz, J. M. Treatise on Materials Science and Technology; Academic Press: New York, 1977; Vol. 10, Part A, p 224.
26. Meeten, G. H. Optical Properties of Polymers; Elsevier Applied Science Publishers: London, 1986; p 289.